



## REMOTE SENSING TECHNOLOGY IN EARTHQUAKE DAMAGE ASSESSMENT

Fumio Yamazaki<sup>1</sup> and Masashi Matsuoka<sup>2</sup>

### ABSTRACT

This paper highlights the recent applications of remote sensing technology in earthquake damage assessment, especially in the 2003 Bam, Iran, earthquake and the 2006 Central Java, Indonesia, earthquake. After the 2003 Bam earthquake, high-resolution satellite images which captured the affected areas before and after the event were fully employed in detailed damage mapping. Various satellite images were also acquired before and after the 2006 Central Java earthquake, and the areas of building damage were extracted based on pixel-based and object-based land cover classifications. In this earthquake, ALOS/PALSAR captured a SAR image of the affected area one day after the event as well as pre-event times. Taking the difference of the pre-event correlation and the pre-and-post event correlation, the areas affected by the earthquake were identified. From these examples, the use of proper satellite imagery is suggested considering the area to cover, sensor type, spatial resolution, satellite's retake time etc., in post-disaster damage assessment.

### Introduction

In the recent few years, large-scale earthquakes and tsunamis brought tremendous damages to urban and rural areas in the world, especially in Asia. It is also pointed out that rapid expansion of urban areas in developing countries has made the areas more vulnerable to various natural disasters. Thus, damage assessments before and after disasters have attracted significant attentions among researchers and practitioners of disaster management. Recent advancements in remote sensing and its application technologies made it possible to use remotely sensed imagery data for assessing vulnerability of an area and for capturing the distribution of damages due to disasters.

To obtain the pre- and post-event spatial information on built and natural environments, several methods exist, such as field survey, airborne remote sensing, and satellite remote sensing. Because of its capacity to cover a vast area in one acquisition time, satellite remote sensing has been a very powerful tool to monitor the condition of the earth surface. High-resolution satellite imagery, which has become available in the last few years, made satellite remote sensing more useful in disaster management since even the damage status of individual buildings and infrastructures can be identified without visiting the sites of disasters.

The present authors have applied the images from QuickBird, the highest resolution commercial optical satellite, to obtain the damage status of individual buildings due to the 2003 Boumerdes, Algeria, earthquake (Yamazaki et al. 2004) and the 2004 Bam, Iran, earthquake (Yamazaki et al. 2005). The recent accumulation of pre-disaster images make post-disaster images more valuable since change (damage) detection can be carried out using them.

---

<sup>1</sup>Professor, Department of Urban Environment Systems, Chiba University, Chiba, Japan, [yamazaki@tu.chiba-u.ac.jp](mailto:yamazaki@tu.chiba-u.ac.jp)

<sup>2</sup>National Institute of Advanced Industrial Science and Technology, Tsukuba, Japan, [m.matsuoka@aist.go.jp](mailto:m.matsuoka@aist.go.jp)

Synthetic Aperture Radar (SAR) is another attractive tool in disaster management because SAR images can be obtained without being affected by weather condition. The present authors have applied SAR intensity images to identify the areas suffered from the collapse of buildings due to earthquakes (Matsuoka and Yamazaki 2004). The change of backscattered echo from severely damaged areas was found to be a useful index to estimate the damage extent and distribution.

In this paper, the applications of satellite imagery to post-disaster damage assessment are demonstrated for the 2003 Bam, Iran, earthquake and the 2005 Central Java, Indonesia, earthquake. The pre- and post-event satellite images are employed as base-maps for field damage survey together with GPS, and they are used in visual and automated damage detection.

## **Damage Detection after The 2003 Bam, Iran, Earthquake**

### **High-resolution satellite images**

After the occurrence of the 26 December 2003 Bam, Iran, earthquake, high-resolution commercial satellites observed the hard-hit areas: Ikonos on 27 December 2003, and QuickBird (QB) on 03 January 2004. The image of the Bam area was also captured by QB on 30 September 2003, about three months before the earthquake. The set of QB images are considered to be the second case acquired by civilian high-resolution satellites both before and after a severe earthquake disaster. The first case was the 21 May 2003 Boumerdes, Algeria, earthquake, and in that case, the images of Boumerdes City were taken about one year before, two days after and 28 days after the event (Yamazaki et al. 2004).

In order to observe target areas in a short time interval, QB can change the view angle of its sensors. Thus, the two images of Bam have different off nadir view angles: 10 degrees (pre-event) and 24 degrees (post-event). Hence it is not so easy to superimpose these images exactly and to perform automated change detection. The difference in building shadow and vegetation in the different acquisition date images gives additional difficulty. Thus visual damage interpretation was performed first. Pan-sharpened images were produced by combining panchromatic images of 0.6m resolution and multi-spectral images of 2.4m resolution, as shown in Fig. 1. By this image enhancement, buildings, cars and debris can clearly be seen.

### **Visual Damage Interpretation of Buildings**

Using the pre-event image, the location of individual buildings was registered on GIS and city blocks surrounded by major roads were assigned. Then visual inspection of building damage was conducted based on the classification in the European Macroseismic Scale (EMS-98; European Seismological Commission 1998), shown in Fig. 2. Comparing the pre- and post-event images, buildings surrounded by debris (Grade 3), partially collapsed buildings (Grade 4) and totally collapsed buildings (Grade 5) were identified.

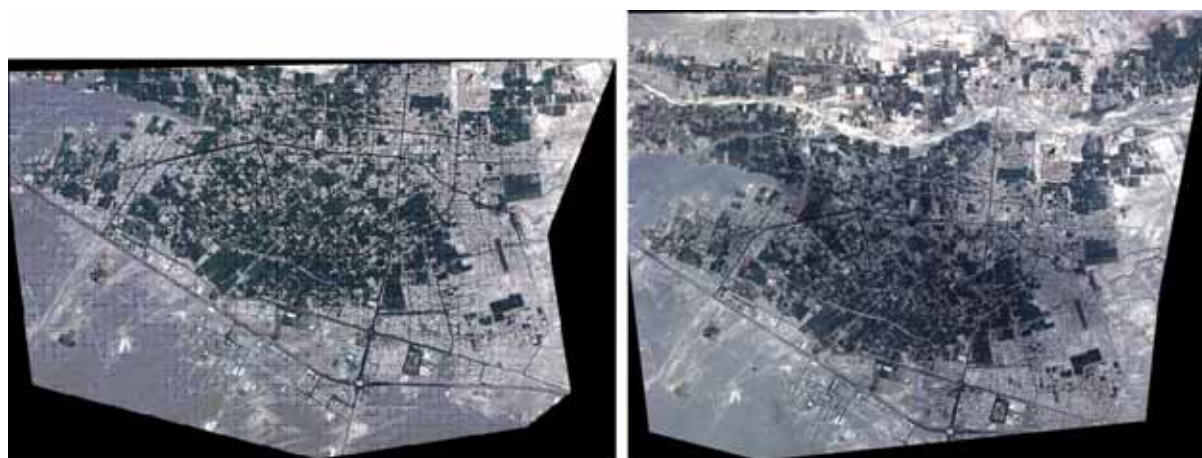


Figure 1. Pan-sharpened natural color QuickBird images of Bam City captured on September 30, 2003 (left: pre-event) and on January 3, 2004 (right: post-event)

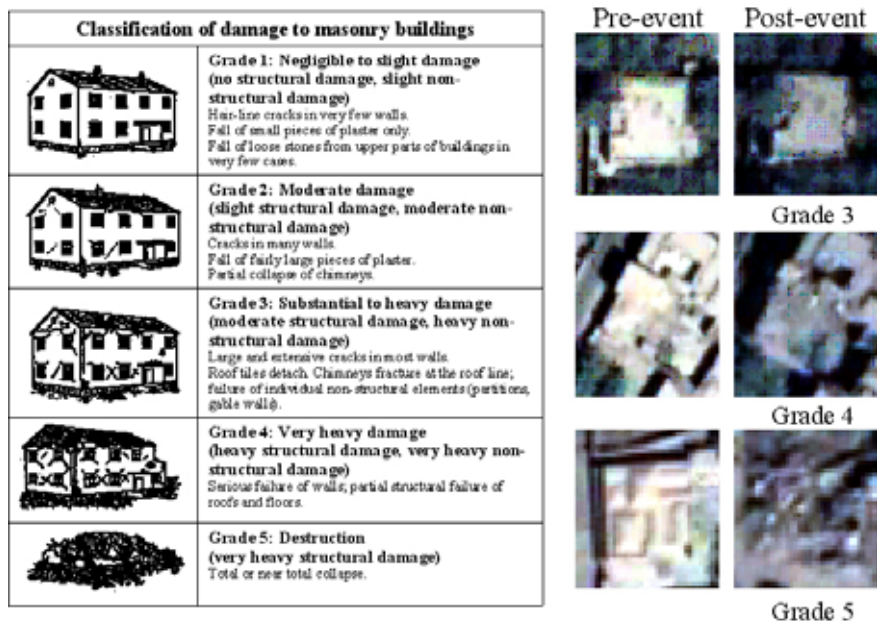


Figure 2. Classification of damage to masonry buildings (EMS 1998) and typical pre- and post event QuickBird images for Grades 3, 4 and 5 houses

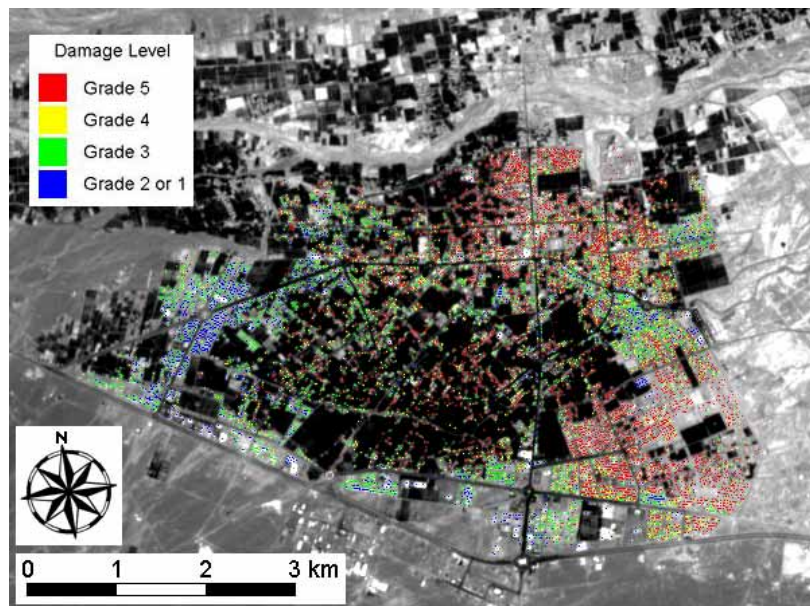


Figure 3. Result of visual damage interpretation using QuickBird images acquired on 30 September, 2003 and 3 January, 2004. Damage levels are based on EMS-98.

In Fig. 2, typical pre- and post-event QuickBird images for houses classified as Grades 3, 4, and 5 by visual inspection are also shown. Because the spatial resolution of the image is around 0.6 m, it is almost impossible to detect damage equal to or less than Grade 2. It is rather easy to detect Grade 5 damage and in agreement among different interpreters was good in case of Grade 5 (Yamazaki et al. 2004). The effects of shadow and vegetation in damage classification become more serious for Grade 4 and damage detection becomes more difficult than that for Grade 5. Damage becomes even more difficult to detect for Grade 3, especially from vertical images. If some deformation is located on the roof or some debris spreads around a building, Grade 3 damage can still be identified.

By this visual interpretation using the pre- and post-event images, a total 12,063 buildings were classified building by building, based on their damage grades, as depicted in Fig. 3. The numbers of identified damaged

buildings are 1,597 (Grades 1 or 2: blue points), 3,815 (Grade 3: green), 1,700 (Grade 4: yellow), and 4,951 (Grade 5: red). The time elapsed to register the location of individual buildings and city blocks using the pre-event image was around 30 hours, and judging and registering the damage grade of each building using the pre- and post-event images was around 20 hours. These elapsed times are considered to be highly dependent on the number of buildings, quality and resolution of images, and experience and efficiency of interpreters.

To examine the accuracy of damage detection in Bam, the field survey data by Hisada et al. (2005) was employed. They used the same EMS-98 scale to describe the damage grade of each building near eight aftershock recording stations, which were established by International Institute of Engineering Earthquake and Seismology (IIEES). Figure 4 shows the satellite image and our visual inspection result around the aftershock seismic station No. 1, together with the cross table between Hisada's survey and our result. Each cell (row, column) in the table shows the number of buildings judged as Grade x (row) in visual interpretation and classified as Grade y (column) in field survey. This area is located in the south of Arg-e-Bam. Sixteen houses were made of mud brick (adobe), and 30 houses were of simple masonry construction. The damage ratio for Grade 5 is 72% by Hisada's survey while it was 64% in our visual inspection. The coincidence of damage grade between the two data sets is quite high in this area.

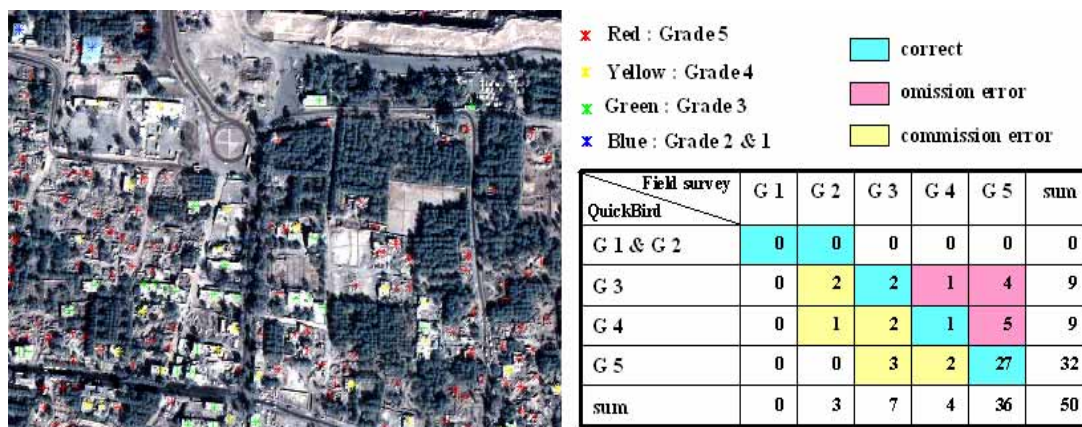


Figure 4. Result of our visual interpretation compared with field survey data by Hisada et al. (2004) around aftershock seismic station No. 1, located in the south of Arg-e-Bam

The result of the field survey around six aftershock observation sites (421 buildings total) in Bam City and that of the visual damage interpretation was compared. Commission errors (judging damage as higher grades than the field survey result) are seen, but only 16 buildings were interpreted as more than one grade higher. Thus, commission error can be judged as not so significant as for quick-look damage detection. Omission errors: judging Grade 4 damage as Grade 1-3, and judging Grade 5 damage as Grade 1-4, are also seen. Forty-two buildings were interpreted as less than one grade lower. It may be concluded that we should expect some amount of omission error in damage detection from optical high-resolution satellite images, and thus we should consider this fact in estimating damage statistics at an early stage.

For the Bam earthquake, the present authors have also conducted an automated damage detection using post-event high resolution satellite imagery (Vu et al. 2005). Moderate resolution optical satellite images (Kohiyama and Yamazaki 2005) and SAR images (Matsuoka and Yamazaki 2005) were also used for damage mapping. For more details, please refer the papers in the references.

## Damage Detection after The 2006 Central Java Earthquake

### The Central Java Earthquake and Field Survey

A strong earthquake of magnitude 6.3 struck Java Island, Indonesia, on May 27, 2006 at 5:54 am local time. The epicenter was located at 7.962°S, 110.458°E, about 25 km south-southeast of Yogyakarta with a fairly shallow focal depth, about 10 km (Figure 5). Due to this earthquake, almost 6,000 people were killed and about 38,000 people were injured. About 140,000 houses were collapsed and about 190,000 houses were heavily

damaged (USGS 2006, UNOSAT 2006).

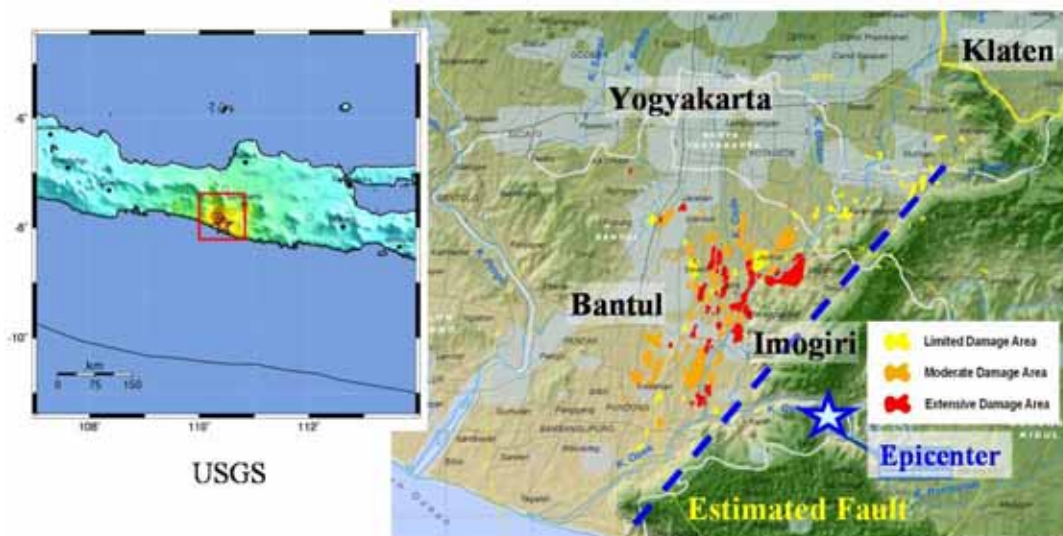


Figure 5. Epicenter of the 2006 Central Java earthquake (USGS 2006) and preliminary damage assessment map produced by UNOSAT (2006) on May 31, 2006.

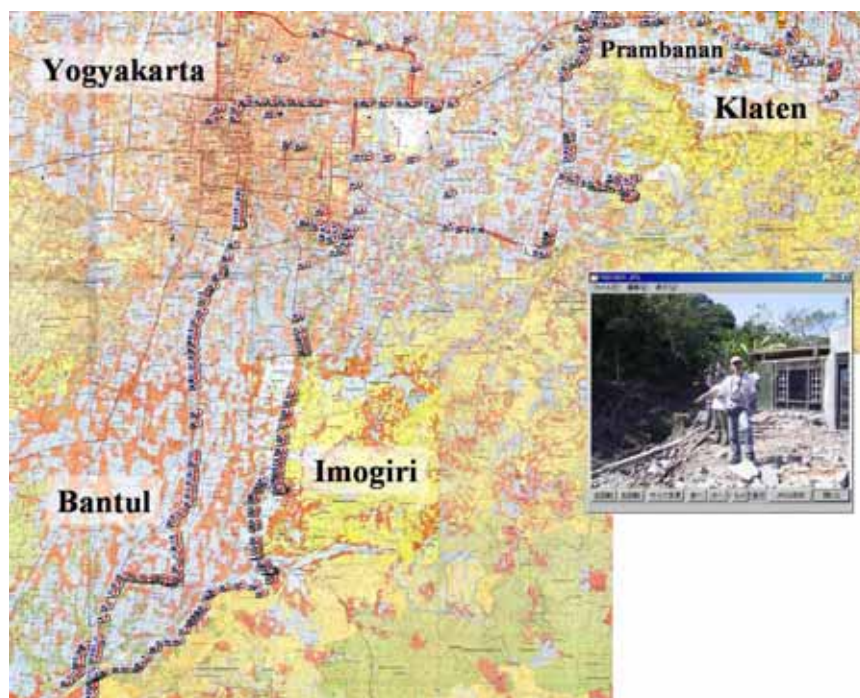


Figure 6. Field survey route by the authors. Camera icons show the locations of GPS synchronized photo shooting.

After the earthquake, various international teams conducted damage surveys of the affected area. As one of sub-teams of the research group supported by the Ministry of Education, Science, Sports and Culture (MEXT), Japanese Government, Grant-in-Aid for Special Purposes, the present authors visited the affected area from 26 to 30 June, 2006. The main objective of our sub-team was to gather geo-referenced ground truth data, which can be used to validate the damage detection results from satellite images. Figure 6 shows the route of the field survey. The camera icons on the map show the locations where we took geo-referenced digital photos.

Figure 7 shows typical damages observed in the field. Figure 7(a) is collapsed brick-masonry houses in a rural area. This type of total collapses of walls and roofs were seen everywhere and considered to be responsible for many casualties in this earthquake in spite of its small magnitude. Figure 7(b) shows a collapsed reinforced-

concrete school building. Such severe damages to engineered buildings were seen only at limited locations. Figure 7(c) shows a large-scale landslide observed in a mountainous area. In Prambanan World Heritage, the largest Hindu temple compound in Indonesia, many big stones were fallen down from the towers as shown in Figure 7(d). The site has been closed to tourists since the earthquake and it was reported that the restoration may take a few years.



Figure 7. Typical damages seen in the field survey: (a) collapsed brick-masonry houses in a rural area, (b) a collapsed reinforced-concrete school building, (c) a large-scale landslide observed in a mountainous area, (d) stones fallen down from the towers in Prambanan temple compound.

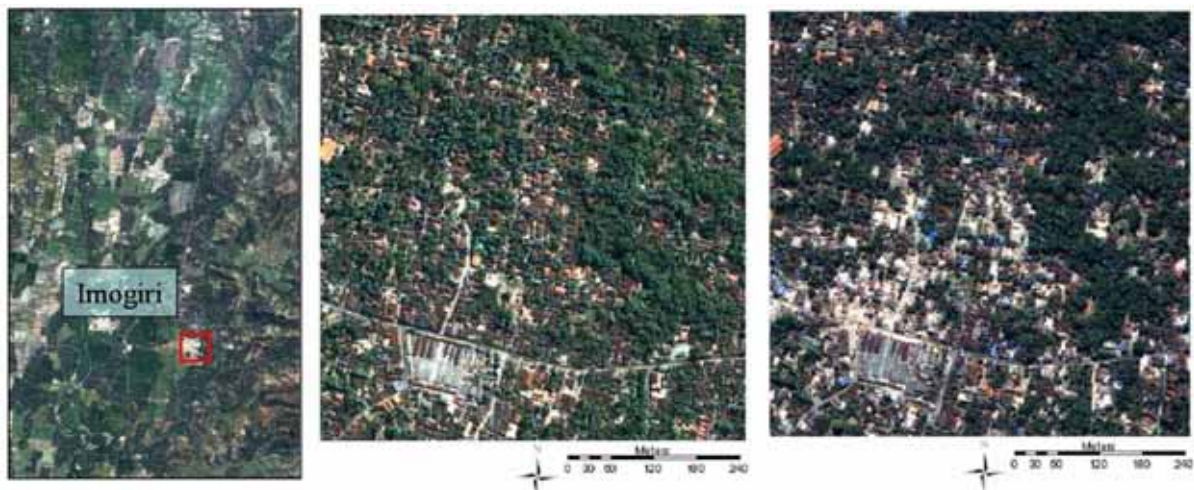


Figure 8. (a) Pan-sharpened natural color QuickBird images of Imogiri area, (b) is the pre-event image and (c) is the post-event image used in this study.

### Damage Detection using QuickBird Images

After the Java Earthquake, QuickBird captured a clear image of the affected areas on June 13, 2006. The image includes Imogiri, one of the most severely affected areas in this earthquake. For the area, a pre-event image captured on July 11, 2003 also exists. Thus a part of these images, shown in Figure 8, were used in this study.

First, a pixel-based classification was carried out based on the maximum likelihood method, the most common

supervised classification method, using 8-bit four bands data. The following 8 classes: black-roof, gray-roof, red-roof, white-roof buildings, road, soil, vegetation, and shadow, were assigned for the pre-event image as the training data. For the post-event image, 7 classes: black-roof, gray-roof, red-roof buildings, debris, road, vegetation, and shadow, were assigned. White-roof building and soil classes were not used for the post-event image because they look close to the debris class and it was difficult to select their training data. The building areas obtained by the pixel-based classification are shown in Figure 9.

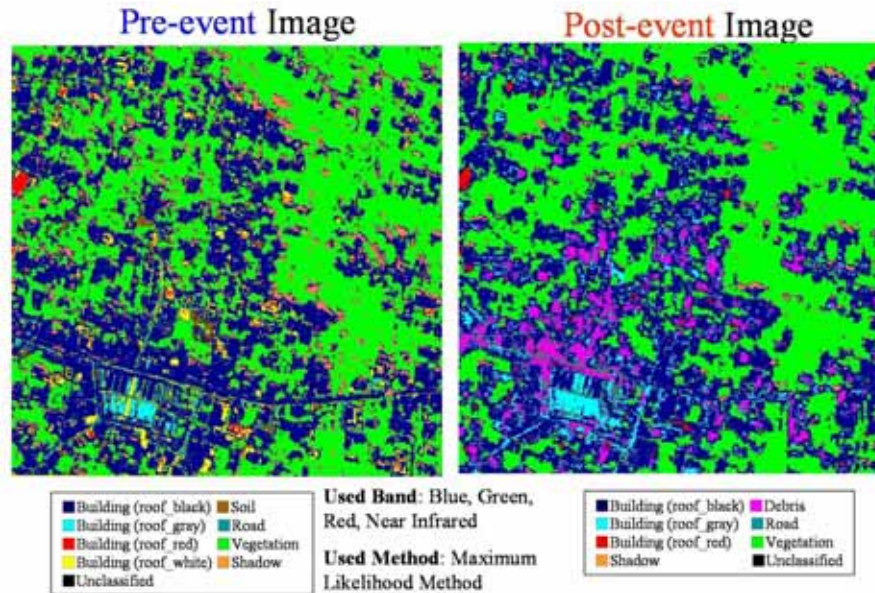


Figure 9. Results of pixel-based land cover classification for pre-event and post-event QB images

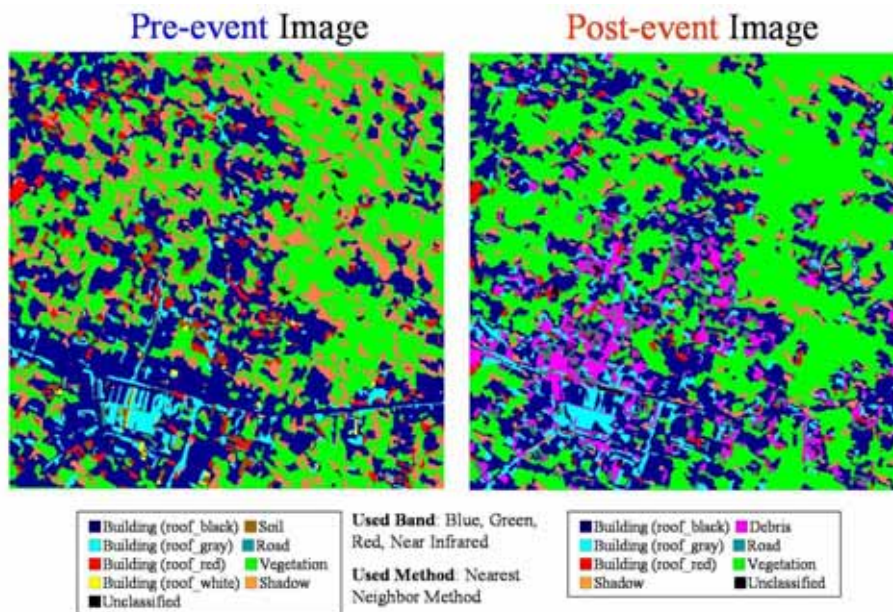


Figure 10. Results of object-based land cover classification for pre-event and post-event QB images

Next, an object-based classification was conducted using e-Cognition software. Image segmentation was carried out as the first step to make “objects” using the pre-event and post-event images. In e-Cognition, the segmentation process is determined by 5 parameters: Layer Weight, Compact Weight, Smooth Weight, Shape Factor, and Scale Parameter (Baatz et al. 2004). The most important parameter is the Scale Parameter, which determines the object size. The Shape Factor is to determine the importance level of spectral heterogeneity or shape heterogeneity in segmentation. The spectral heterogeneity is decided by Layer Weight, which gives the weight for each band. The shape heterogeneity is decided by Compact Weight and Smooth Weight. The bigger

the Compact Weight is, the segmented objects are in a more compact shape. Starting from pixels, segmentation runs the merge between two objects and is terminated when an assigned condition is reached. Although it is difficult to decide the appropriate parameters values suitable to all land cover classes, the user can decide the suitable values to a few focused classes, e.g. building, road.

The results from the object-based classification for the pre-event and post-event images are shown in Figures 10. Comparing the results from the pixel-based and object-based classifications with that by visual inspection, salt-and-paper noises are seen in the pixel-based classification. Hence, it may be concluded that in this high resolution and the sizes of the target objects, the better result can be acquired by object-based classification. But in object-based classification, some road and shadow areas were misclassified to building classes because their spectral values of the sample area are similar to those of building classes. Hence even object-based classification, some classes like these are needed to remove in advance using object feature indices, e.g. length, or spatial relationships.

### Damage Detection using ALOS/SAR Images

The Advanced Land Observing Satellite (ALOS, “Daichi” in Japanese), was launched successfully on January 24, 2006, by the Japan Aerospace and Exploration Agency (JAXA). After providing first shots captured by the onboard sensors, PRISM, AVNIR-2, and PALSAR (Phased Array Type L-band Synthetic Aperture Radar), ALOS has been performing the image acquisition of natural disasters at an early stage, such as the mudslide occurred in Leyte Island, the Philippines, on February 17, 2006, the volcanic eruptions of Mt. Merapi, Indonesia, from April to May 2006, and the flood in north Thailand on May 2006.

A good quality image of the affected areas was captured by PALSAR one day after the 27 May 2006 Central Java earthquake. Fortunately, time-series pre-event PALSAR images have already been acquired and available to use in change (damage) detection because the earthquake source and the affected areas are located rather near Mt. Merapi volcano. In this study, two pre-seismic images (April 29 and May 16, 2006) and one post-seismic image (May 28, 2006) were employed for the affected areas such as Bantul and Yogyakarta regions and applied them in change detection, evaluating the difference in pre- and co-seismic correlations.

By activating the disaster charter (International Charter 1999), L-band SAR system, PALSAR (HH polarization with 9m resolution) onboard ALOS, was operated for capturing the information on the areas damaged due to the earthquake. Figure 11 shows the backscattering intensity images of time-series PALSAR covering Yogyakarta and central Java provinces. On the next day of the earthquake, PALSAR observed the area successfully in 36.9 degree off-nadir angle (microwave transmission angle). Two pre-event images had also been obtained on April 29 and May 16, 2006 with 34.3 and 30.8 degree off-nadir angles, respectively.

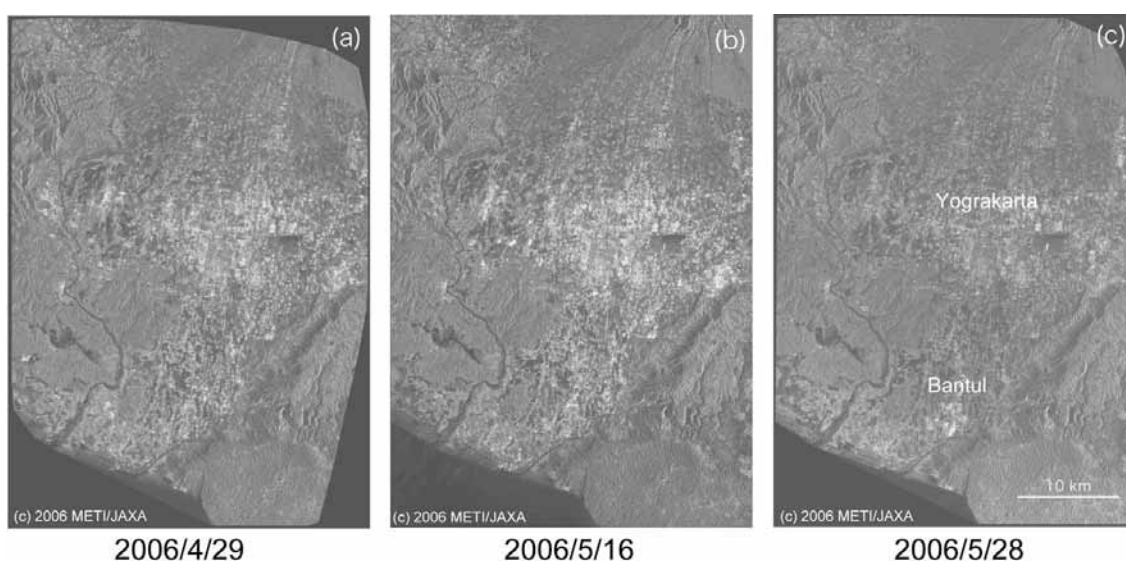


Figure 11. Backscattering intensity images of Yogyakarta area from ALOS/PALSAR before and after the 27 May 2006 Central Java earthquake.

Using these images, the variation of the correlation coefficient was calculated and the effects of signal noise and stationary temporal changes were evaluated. The distribution of the difference,  $r_{diff}$ , between the  $r_{bb}$  value of the two pre-event images and the  $r_{ab}$  of the pre- and post-event images plotted on PALSAR intensity image is shown in Figure 12 (a). To focus on built-up areas, the decorrelated areas (correlation coefficient less than 0.8) from the pre-event pair were excluded from the analysis in advance. In Bantul, the lower  $r_{diff}$  areas distribute from southwest to northeast, showing good agreement to the estimated damaged areas (see Figure 5) by visual interpretation from high-resolution satellite images (UNOSAT 2006).

A Japanese field survey team carried out an intensive building damage investigation around schools and obtained the ratio of severely damaged buildings in a 500 m radius from a school (Maeda et al. 2007). In Figure 12 (a), twelve investigated areas (colored-circles classified by the severely damaged ratio) are also plotted on the  $r_{diff}$  distribution.

For a quantitative analysis, we selected pixels within the investigated circles in the field survey and calculated the average and standard deviation of  $r_{diff}$  value in each damage level. The damage levels classified into D, E, and F, correspond to the severely damaged ratio of 25-50, 50-75, and 75-100 %, respectively. The comparison between the building damage level and the difference in correlation coefficient,  $r_{diff}$ , is shown in Figure 12 (b). The numbers on the top of the error bars represent the counts of pixels. In the figure, as the damage level increases, the difference in the correlation coefficient is seen to decrease although the standard deviation is quite large. The similar trend was also observed in SAR intensity images from several damaging earthquakes (Matsuoka and Yamazaki 2004, 2005).

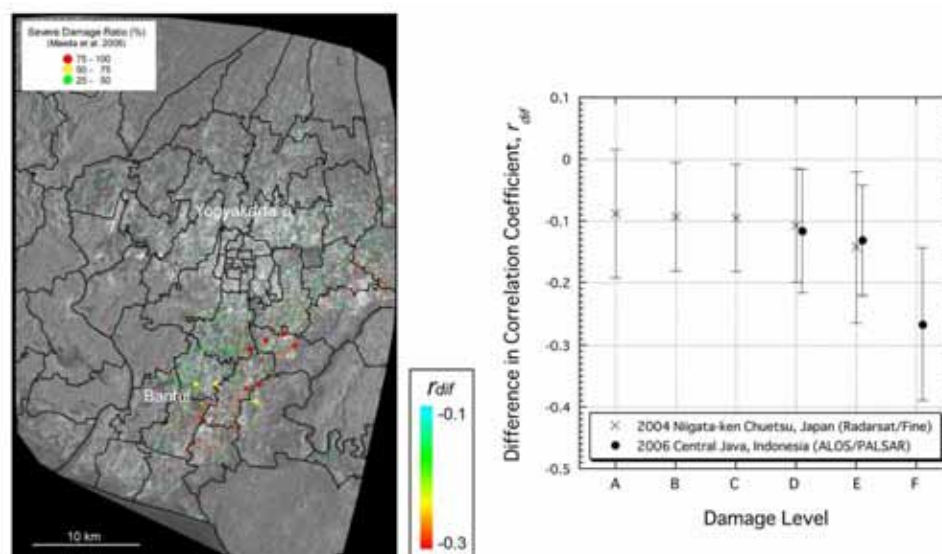


Figure 12. (a) Distribution of the difference,  $r_{diff}$ , between correlation coefficients derived from ALOS/PALSAR imagery, plotted on the post-earthquake backscattering intensity image. The colored circles indicate the building damage ratio surveyed by Maeda et al. (2007). (b) Relationship between the building damage level and the difference between correlation coefficients,  $r_{diff}$ . The results of similar study for the 2004 Mid-Niigata earthquake (Matsuoka et al. 2007) are also shown for comparison.

## Conclusions

The recent applications of remote sensing technologies in post-disaster damage assessment were highlighted using the satellite imagery obtained in the 2003 Bam earthquake and the 2006 Central Java earthquake, as typical examples. Using high-resolution satellite images of Bam City acquired by QuickBird before and after the Bam earthquake, visual interpretation of building damage was carried out. Comparing the pre-event and post-event pan-sharpened images, buildings surrounded by debris, partially collapsed buildings, and totally collapsed buildings were identified based on the European Macroseismic Scale.

After the 2006 Central Java earthquake, high-resolution optical satellite images were fully employed to extract the areas of severe building damage. In our field investigation, satellite images were used as base-maps together with GPS. Comparing the pre-and post-event QuickBird images, the areas of severe building damage were extracted based on pixel-based and object-based classifications and their accuracy was compared with visual inspection results. In the Java earthquake, ALOS/PALSAR captured a SAR image of the affected area one day after the event as well as pre-event times. Taking the difference of the pre-event correlation and the pre-and-post event correlation, the areas affected by the earthquake were also extracted in good accuracy.

In summary, satellite images can be used efficiently in post-disaster damage assessment if they are selected properly in terms of sensor type (optical or SAR), spatial resolution, satellite's retake time, and the availability of pre-event images and digital maps, etc.

## Acknowledgments

This study was partially supported by the Ministry of Education, Science, Sports, and Culture, Grant-in Aid for Special Purpose No.1890001 (Representative: Prof. H. Kawase of Kyushu University). The research outputs introduced in this paper have been produced by Dr. T. T. Vu, Mr. Y. Yano, and Mr. K. Matsumoto of Chiba University. Their contributions are deeply appreciated. The field survey data of Bam was provided from Prof. Y. Hisada of Kogakuin University and Dr. A. Shibayama of Tohoku University. QuickBird images of Bam were licensed and provided by Earthquake Engineering Research Institute (EERI), Oakland, California, USA. ALOS data was provided from the Japan Aerospace Exploration Agency (JAXA) under collaborated research.

## References

- Baatz, M., Benz, U., et al., 2004. *e-Cognition user guide 4*, Definiens Imaging, 76-78.
- European Seismological Commission, 1998. *European Macroseismic Scale 1998*.
- Hisada, Y., Shibayama, A., and Ghayamghamian, M.R., 2005. Building damage and seismic intensity in Bam City from the 2003 Iran, Bam, Earthquake, *Bulletin of Earthquake Research Institute*, University of Tokyo, Vol. 79, No. 3 & 4, pp. 81-94.
- International Charter, 1999. Space and Major Disaster, <http://www.disasterscharter.org/>.
- Kohiyama, M., and Yamazaki, F., 2005. Damage Detection for 2003 Bam, Iran, Earthquake Using Terra-ASTER Satellite Imagery, *Earthquake Spectra*, 21(S1), S267-S274.
- Maeda, M. et al., 2007. Damage of School Buildings and Residential Houses, *Report on the Damage Investigation of the 2006 Central Java Earthquake*, Architectural Institute of Japan.
- Matsuoka, M. and Yamazaki, F., 2004. Use of satellite SAR intensity imagery for detecting building areas damaged due to earthquakes", *Earthquake Spectra*, 20 (3), 975-994.
- Matsuoka, M. and Yamazaki, F., 2005. Building damage mapping of Iran earthquake using Envisat/ASAR intensity imagery, *Earthquake Spectra*, 21(S1), S285-S294.
- Matsuoka, M. and Yamazaki, F. and Ohkura, H., 2007. Damage mapping for the 2004 Niigata-ken Chuetsu earthquake using Radarsat images, *2007 Urban Remote Sensing Joint Event*, IEEE, Paris, France, CD-ROM.
- UNOSAT, 2006. Indonesia Maps, <http://unosat.web.cern.ch/unosat/asp/>.
- USGS, 2006. <http://earthquake.usgs.gov/eqcenter/eqinthenews/2006/usneb6/>
- Vu, T. T., Matsuoka, M., and Yamazaki, F., 2005. Detection and Animation of Damage Using Very High-Resolution Satellite Data Following the 2003 Bam, Iran, Earthquake, *Earthquake Spectra*, 21( S1), S319-S327.
- Yamazaki, F., Kouchi, K., Matsuoka, M., Kohiyama, M., and Muraoka, N., 2004. Damage Detection from high-resolution satellite images for the 2003 Boumerdes, Algeria Earthquake, *Proceedings of the 13th WCEE*, CD-ROM, Paper No. 2595.
- Yamazaki, F., Yano, Y., and Matsuoka, M., 2005. Visual damage interpretation of buildings in Bam city using QuickBird images, *Earthquake Spectra*, 21( S1), S329-S336.